Multiphysics Dynamic Model Validation Methodology for Laser-Driven Microrobots

Zhong Yang, Mohammad N. Saadatzi, Ruoshi Zhang, Andriy Sherehiy,
Danming Wei, Cindy K. Harnett, and Dan O. Popa[1]

Abstract—**In this paper we discuss a comprehensive multi-physics modeling and simulation approach with experimental validation, aimed at understanding the behavior of laser-driven microrobot locomotion on two-dimensional (2D) substrates. The ChevBot is a novel class of light actuated sub-millimetric microrobots that can perform tasks equivalent to mobile robots in future microfactories for nano-bio-technology. The robot dynamics is driven by a complex photo-thermo-mechanical conversion mechanism and stick-and-slip locomotion, which are difficult to simulate. Therefore, 1D and 2D reduced order models are proposed to approximate the microrobot dynamics. Models are then validated using a combination of Finite Element Analysis simulations and direct experimentation. The framework presented here automates the process of collecting motion tracking data from microrobots and uses it to validate dynamic models. In the future, our models can be used in subsequent closed-loop control and design optimization studies.**

I. INTRODUCTION

Microrobotics has received a lot of attention in the last few decades due to a myriad of applications in medicine such as drug delivery, cell injection, surgery, etc., and in nanotechnology, such as nanomanipulation, characterization of new materials and microscopy. Several research groups have studied locomotion mechanisms for microrobots based on harvesting ambient fields to produce controlled motion on the micro and nanoscales. These fields include electrostatic, magnetic, electromagnetic, laser and ultrasonic vibration energy delivered to mobile agents with sizes below 1 mm. Among remote actuation methods, magnetic fields have traditionally been among the most widely employed. In [1,2] electromagnetic fields were harvested to drive micromagnetic robots, in which the modulated field directly supplies driving force and moments. In general, the theory of operation for magnetic microrobots is well understood and is often used to accomplish closed-loop control, as well as serve as a design aid during robot fabrication [3],[4]. In [5] the electromagnetic field was used to levitate microrobots, and a laser beam was introduced to open and close a microgripper.

Laser actuation of microrobots is a remote powering method that has limitations due to its directional nature and requires simultaneous tracking control with the microrobot in motion. The Robofly [6] is an example of a microrobot's use of laser light as a source of energy to power a piezoelectric drive. Utilizing laser as both power and control source is a relatively newer idea, so far realized on bubble microrobots with thermal gradients [7], and in optical trapping and tweezing [8]. However, these examples are limited to operation in liquid environments due to limited force output of their drive mechanisms.

The Chevbot, first introduced in [9], is a novel locomotor that uses light energy harvesting inducing thermal effects that generate motion in dry-environments. The microrobot drive consists of Chevron Thermal Actuators (CTA), which are popular Micro Electro Mechanical (MEMS) drive systems [10]. The CTA is powered by laser beam energy directly from a 532nm green Nd:Yag laser source, and produces stick and slip crawling locomotion on the 2D substrate. In order to optimize the geometry of the microrobot, and to accomplish controlled motions on a variety of substrates, ChevBot reduced-order multiphysics simulation models need to be developed. However, unlike magnetic microrobots, ChevBots convert optical to thermal to mechanical energy, conversion phenomena that depend on the geometry and material properties of both robot and environment. Although thermo-mechanical dynamical conversion models for MEMS electrothermal actuators are well-established [11,12], stick-and-slip models are much more complex [13], while opto-thermal conversion models from laser energy have received very little coverage in scientific literature.

The contribution of this paper is to put forth a comprehensive methodology for constructing lumped opto-thermo-mechanical models of laser-driven microrobots. An experimental data collection system was used to automate the process of laser power delivery to the microrobots and perform system identification while tracking the robot motion. Simulation results using Finite Element Methods were used to compare the operating performance and the thermal time constant of ChevBots in two different operating conditions: one in which the robots are tethered to the MEMS substrate, and one in which they freely move on the 2D substrate. Experimental motion profiles collected with a laser range sensor were used to validate the dynamics of actuation and construct reduced order models of the CTA. A 1D dynamic model of ChevBot was then proposed, and tuned to experimentally collected data. The model was then extended in 2D to study the expected motion of the robot under varying friction conditions. In future work, such models can be used

[1] Authors are with the Department of Electrical and Computer Engineering, University of Louisville, Kentucky, USA.

for microrobot design optimization, as well as closed-loop control synthesis.

The paper is organized as follows: in Section II we describe the ChevBot microrobots and their locomotion principle. In Section III, we introduce proposed opto-thermo-mechanical models, discussing both Finite Element (FEA) models and lumped 1D and 2D dynamic models. in section IV, we implement these models to obtain simulations; while in section V we present validation experiments for the proposed models; finally, section VI concludes the paper and discusses future work.

II. Robot Description and Locomotion Principle

The ChevBot is a MEMS-based microrobot, fabricated from a silicon-on-insulator (SOI) wafer with 20µm device layer, to which as microassembled dimple is added using a microassembly system located in our lab. As shown in Fig. 1, ChevBots consist of four components, namely a body frame, the CTA actuator, a set of "feet", and the assembled dimple under the frame. Conventional CTAs are powered by voltage or current sources and generate thermal expansion and mN-size forces by Joule heating. In our microrobot, the actuator is powered directly from a laser beam, which can be focused on a part or on the whole robot. In the first case, it may be possible to locally affect the temperature gradient in selected parts of the microrobot, while in the latter case, it will be easier for the laser beam to track the robot while in motion. As the CTA absorbs energy from laser beam, it generates thermal expansion, which, when combined with a stick-slip motion of the feet will create locomotion on a flat substrate.

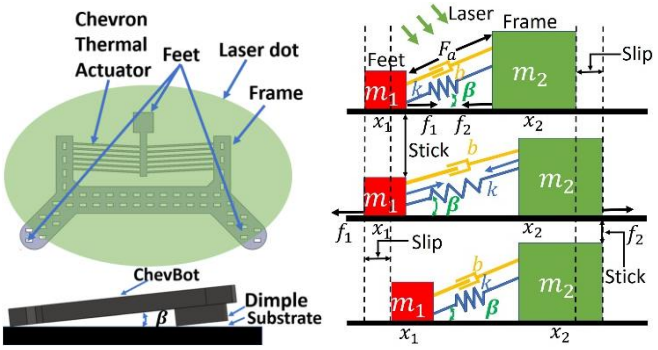

Figure 1 (Left) Top and side view of an untethered ChevBot fabricated from a 20 µm device layer SOI substrate. The scale bar is 100 µm. (Right) Free Body Diagram of ChevBot explaining the stick-slip actuation cycle from pulsed laser beam.

In a typical design and fabrication process detailed in [9], ChevBots measured approximately 750µm in width and 425µm in length, and with an assembled dimple, its total thickness is 40µm. Each of the 12 beams in the CTA is 5µm wide and they form an acute angle θ with the body frame. In Fig. 1, the green ellipse represents the laser spot with large waist diameter of 800µm and small waist diameter of 600µm, corresponding to the experimental conditions After the dimple is assembled, the ChevBot is inclined by a small angle β to the substrate, and moves according to a stick and slip cycle induced by the pulsed laser beam. The inner edge of the rectangular-shaped dimple and the tail act as three contact edges to the substrate.

In the "laser on" part of the actuation cycle the body/dimple sticks to the substrate due to static friction conditions, while the feet slip via CTA actuation. In the "laser off" part of the actuation cycle, caused by variations in the robot tilt angle β, the feet stick to the substrate, while the body slips creating a net velocity.

III. Photo-Thermal-Mechanical Models

Modeling the Chevbot is a multiphysics problem, in which an energy transfer process is initiated when laser is focused onto the CTA. Laser energy is absorbed in the robot frame and actuator, and converter into heat. Directional thermal expansion on the actuator will generate the driving force and displacement on the microrobot feet and dimple. Then, static and dynamic friction/stiction forces will lead to stick-slip locomotion. The resulting Photo-Thermal-Mechanical process is shown in Fig.2, in which the three conversion components, and their corresponding physical phenomena and boundary conditions are indicated. The figure also depicts the thickness of various layers involved in the associated heat transfer problem.

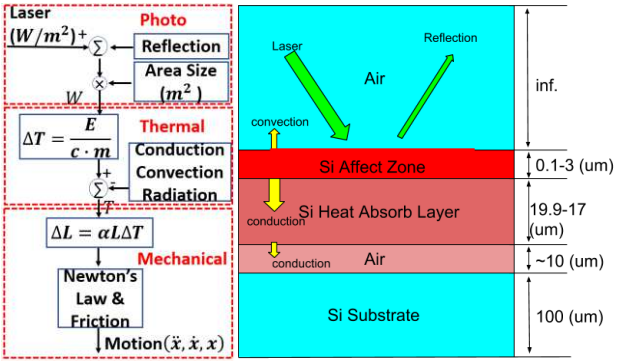

Figure 2 Photo-Thermal-Mechanical conversion for ChevBots, and representative layer thickness of the robot geometry.

A. Photo-Thermal Model

The Photo-Thermal model describes the behavior of the robot transferring light to heat energy. In this process, some of light energy is reflected on the microrobot surface, while the rest is absorbed to generate heat dissipated by thermal conduction, air convection and radiation. If enough time elapses, the temperature on the CTA will reach an equilibrium, and a steady-state displacement. If the temperature stays bounded below normal operating conditions for CTAs, radiation and convection are typically much smaller than conduction, and can be neglected [13]. From the conservation law of energy, we have:

$$dQ_{laser} - dQ_{ref} - dQ_{cond} = dQ_{st}, \qquad (1)$$

where dQ_{laser} is the energy generated by the laser, dQ_{ref} is the energy lost by surface reflection, dQ_{cond} is the energy lost by conduction, and dQ_{st} is the energy storage in the thermal actuator, which will generate thermal expansion. By expanding terms in this equation through Newton's law of cooling, we obtain a first order differential equation describing the CTA's average temperature T as a lumped model [15]:

$$(1 - R)E_e A_l - hA_r(T - T_\infty) = \rho V c \frac{dT}{dt}, \qquad (2)$$

in which R is the surface reflectivity, E_e is the laser irradiation, A_l is the laser spot heating area, h is the thermal conductivity constant, A_r is the thermal actuator area, T_∞ is the environment temperature, ρ is the material density, V is the volume of the actuator and c is the specific heat capacity of the microrobot material.

B. Thermal Expansion and Displacement of the CTA

Eq. (2) drives the actuator temperature and is the source of thermal expansion generating both displacement and driving force of the microrobot's CTA. The thermal expansion length ΔL can be written as:

$$\mathrm{d}L = \alpha L \mathrm{d}T, \tag{3}$$

where the α is the thermal expansion coefficient, $\mathrm{d}T$ is the temperature change on the thermal actuator, and L is the original length actuator beams. Furthermore, the relation between thermal expansion $\mathrm{d}L$ to the displacement d_T of the CTA can be calculated by:

$$d_T = \sqrt{[L^2 + 2L(\mathrm{d}L) - Lcos^2(\theta)]} - Lsin(\theta), \tag{4}$$

where the θ is the angle of the bent beam of the CTA. Finally, the relationship between displacement of actuator Δd_T and force F_a on the actuator is given by [12]:

$$F_a = \frac{2NAEsin^2(\theta)}{L} d_T, \tag{5}$$

where N is the number of beams of the Chevron actuator, A is cross section area of the beams, E is Young's modulus.

C. 1-D Spring and Damper model of the ChevBot

By lumping the mass of the robot frame into mass m_2 and the mass of the CTA and feet into mass m_1, we can describe a 1D dynamic model for the microrobot according to the free body diagram of Fig. 1 (right). When the laser is on, a CTA force Fa given in eq. (5) is applied on the spring mid-section of the robot. This force will be projected onto the horizontal and vertical directions and result in varying friction forces as a function of tilt angle β. The spring-mass-damper system has two degrees of freedom x_1 and x_2, resulting in two equations according to force equilibrium along the horizontal x axis. For actuator and feet, this becomes:

$$-F_a \cos\beta + k\left(\frac{x_2 - x_1}{\cos\beta} - l_0\right)\cos\beta - \mathrm{sign}(\dot{x}_1) f_1 + b(\dot{x}_2 - \dot{x}_1) = m_1 \ddot{x}_1, \tag{6}$$

while for robot body and dimple it is:

$$F_a \cos\beta - k\left(\frac{x_2 - x_1}{\cos\beta} - l_0\right)\cos\beta - \mathrm{sign}(\dot{x}_2) f_2 - b(\dot{x}_2 - \dot{x}_1) = m_2 \ddot{x}_2. \tag{7}$$

In the dynamical equations, (6) and (7), k and b represent the actuator stiffness and viscous damping coefficients, while l_0 is the initial actuator length. Furthermore, the friction forces are expressed from the resultant of vertical forces accruing on masses m_1 and m_2 respectively, expressed by a Stribeck Friction model given by:

$$f_1 = \mu\left(m_1 g + \left(-F_a \sin\beta + k\left(\frac{x_2 - x_1}{\cos\beta} - l_0\right)\sin\beta\right)\right) - k_v \dot{x}_1, \tag{8}$$

$$f_2 = \mu\left(m_2 g - \left(F_a \sin\beta - k\left(\frac{x_2 - x_1}{\cos\beta} - l_0\right)\sin\beta\right)\right) + k_v \dot{x}_2 \tag{9}$$

where $\mu \in \{\mu_s, \mu_d\}$, μ_s is static friction constant. μ_d is the dynamic friction constant, depending on the pushing force F_a and the friction regime, k_v is a viscous friction constant. h_d is the dimple height. The tilt angle β can be expressed by:

$$\beta = \tan^{-1}\frac{h_d}{x_2 - x_1} \tag{10}$$

The Stribeck friction model is a combination of Coulomb friction and viscous friction and was shown to be accurate in predicting the average speed of microscale stick and slip motion, but not i accurately predicting the instantaneous velocity of the microrobot legs [12]. In particular, the velocity of dimple or leg in the "stuck" phase will not be zero as needed. Although other stick-slip models such as LuGre can be applied for more accurate leg motion prediction, here we avoid additional modeling complexity by switching the stick and slip conditions of the leg and body according to a velocity threshold constant ε in the algorithm below:

Algorithm 1: Stick- Slip motion calculation

For i=1,2
if *Force applied > static friction force on mass m_i*
Output current velocity v_i calculated by acceleration integration of eq. (6) or (7) with dynamic friction coefficient.
else if $|v_i| < \varepsilon$
Set v_i velocity to zero
else
Output current velocity v_i calculated by acceleration integration of eq. (6) or (7) with dynamic friction coefficient.
Calculate x_i location by integrating velocity v_i.
end

D. 2-D model of the ChevBot

We can expand the 1D dynamical model of the microrobot by considering the three points/lines of contact with the substrate referring to the free body diagram in Fig. 3.

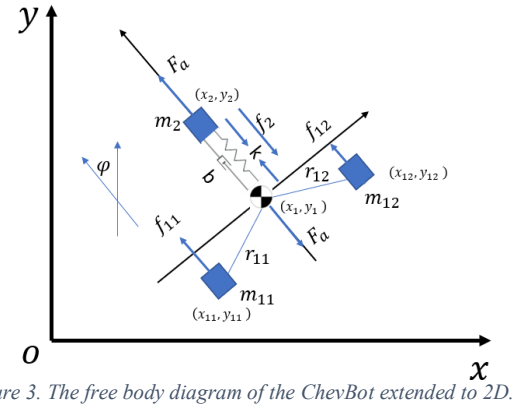

Figure 3. The free body diagram of the ChevBot extended to 2D.

The CTA actuator can generate forces and push the robot to move forward or backward, while the friction force unbalance will generate a torque causing rotations. Thus, the ChevBot will behave similarly to a differential drive robot and is susceptible to uneven friction/stiction forces and uncertainty of touching surfaces on the substrate. A 2D extension of the

model in equations (6) and (7) will have an additional equation of motion summarized in vector form notation:

$$\boldsymbol{F_a} - \boldsymbol{f_2} - k(\boldsymbol{x_2} - \boldsymbol{x_1} - \boldsymbol{R}\cdot\boldsymbol{l_0}) - b(\dot{\boldsymbol{x}}_2 - \dot{\boldsymbol{x}}_1) = m_2\ddot{\boldsymbol{x}}_2, \quad (11)$$

$$-\boldsymbol{F_a} + \boldsymbol{f_{11}} + \boldsymbol{f_{12}} - k(\boldsymbol{x_1} - \boldsymbol{x_2} - \boldsymbol{R}\cdot\boldsymbol{l_0}) - b(\dot{\boldsymbol{x}}_1 - \dot{\boldsymbol{x}}_2) = (m_{11} + m_{12})\ddot{\boldsymbol{x}}_1, \quad (12)$$

$$I\ddot{\varphi} = \boldsymbol{r_{11}} \times \boldsymbol{f_{11}} + \boldsymbol{r_{12}} \times \boldsymbol{f_{12}}, \quad (13)$$

where bolded quantities are 2 dimensional vectors, $\boldsymbol{f_2}$ is the friction force on the dimple, $\boldsymbol{f_{11}}$ and $\boldsymbol{f_{12}}$ are the friction forces on two microrobot feet, $\boldsymbol{r_{11}}$ and $\boldsymbol{r_{12}}$ are the positional vectors from friction forces $\boldsymbol{f_{11}}$ and $\boldsymbol{f_{12}}$ to the center of the mass of the ChevBot and $\boldsymbol{R}$ is rotational matrix from ChevBot local frame to the global frame. In a 2-D scenario, the ChevBot has 5 degrees of freedom in total, and the equations of motion (11)-(13) can be expanded as:

$$\begin{pmatrix}F_{ax}\\F_{ay}\end{pmatrix} - \begin{pmatrix}f_{2x}\\f_{2y}\end{pmatrix} - k\left[\begin{pmatrix}x_2\\y_2\end{pmatrix} - \begin{pmatrix}x_1\\y_1\end{pmatrix} - \begin{pmatrix}\cos\varphi & -\sin\varphi\\ \sin\varphi & \cos\varphi\end{pmatrix}\begin{pmatrix}l_0\\0\end{pmatrix}\right] - \mathrm{b}\begin{pmatrix}\dot{x}_2 - \dot{x}_1\\ \dot{y}_2 - \dot{y}_1\end{pmatrix} = m_2\begin{pmatrix}\ddot{x}_2\\\ddot{y}_2\end{pmatrix}, \quad (14)$$

$$-\begin{pmatrix}F_{ax}\\F_{ay}\end{pmatrix} + \begin{pmatrix}f_{11x}\\f_{11y}\end{pmatrix} + \begin{pmatrix}f_{12x}\\f_{12y}\end{pmatrix} - k\left[\begin{pmatrix}x_1\\y_1\end{pmatrix} - \begin{pmatrix}x_2\\y_2\end{pmatrix} - \begin{pmatrix}\cos\varphi & -\sin\varphi\\ \sin\varphi & \cos\varphi\end{pmatrix}\begin{pmatrix}l_0\\0\end{pmatrix}\right] - \mathrm{b}\begin{pmatrix}\dot{x}_1 - \dot{x}_2\\ \dot{y}_1 - \dot{y}_2\end{pmatrix} = (m_{11} + m_{12})\begin{pmatrix}\ddot{x}_1\\\ddot{y}_1\end{pmatrix}, \quad (15)$$

$$I\ddot{\varphi} = -r_{11}f_{11y}\cos\theta_{11} + r_{11}f_{11x}\sin\theta_{11} - r_{12}f_{12y}\cos\theta_{12} + r_{12}f_{12x}\sin\theta_{12}, \quad (16)$$

where F_{ax} and F_{ay} are the components of F_a, f_{2x} and f_{2y} are the components of friction force on dimple, f_{11x}, f_{11y}, f_{12x} and f_{12y} are the components of friction force on feet, x_1 and y_1 are the position of the dimple, x_2 and y_2 are the position of the center of the mass of the microrobot. m_{11} and m_{12} are the mass distributed on feet, the m_2 is the mass distribute on dimple. r_{11} and r_{12} are the distance of masses distribute on legs relative to the mass of center, I is angular moment of inertia, φ is the microrobot orientation angle, θ_{11} and θ_{12} are the angle configuration of the feet relative to the center of the mass, k and b are the CTA spring constant and damping coefficients, respectively.

IV. Simulation Results

A. Opto-Thermal Finite Element Analysis

To better understand the thermal behavior and stiffness of the actuator of the ChevBot, we conducted a series of Finite Element Analysis (FEA) Multiphysics simulations. Although many FEA packages, such as ANSYS® offer computing engines for coupled thermal, mechanical, magnetic, piezoelectric, etc., effects, they do not simulate laser radiation absorption. To simulate photo-thermal behavior in our study the absorption of laser energy can be approximated. Specifically, we calculate a heat reception (HAZ) layer on the top surface of the ChevBot, and then implement this layer via "Internal Heat Generation" boundary conditions. The HAZ thickness is given by Beer-Lambert's law written as [16]:

$$e^{-\alpha z} = 0.1, \quad (17)$$

where the α is the absorption coefficient, and 0.1 means 90 percent of the transmitted light is absorbed below depth z. In our case, using Si material absorption constant $\alpha = 10197.2(cm^{-1})$ for a green 532nm laser [15], a resulting 2μm thick HAZ layer with a rectangular shape representing the laser spot was sliced on the device layer. An ANSYS® model was built to simulate a 780μm × 510μm tethered microrobot block, with all vertical structures corresponding to the handle layer, the buried oxide, and 2μm air gap between release and the device layer. FEA simulations were conducted using an irradiance of 1.9995e7 W/m^2 directed at the microrobot as shown in Fig. 4. This irradiance value is similar to the energy of the laser beam used in experiments.

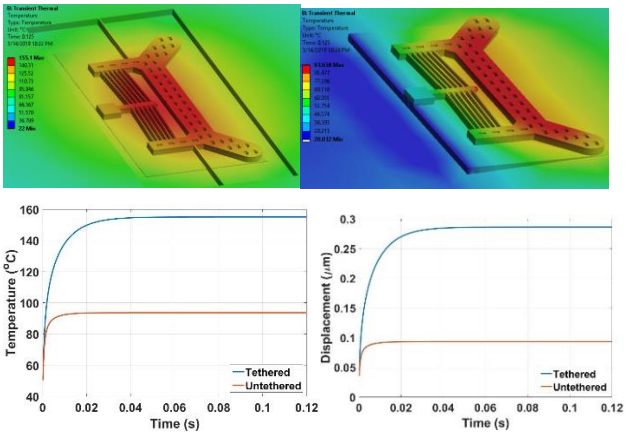

Figure 4 ANSYS® Thermo-mechanical simulation for shuttle displacement and temperature distribution of ChevBots tethered (left-top), and untethered (right-top). Graphs correspond to maximum temperature (left) and displacement (right).

The boundary conditions of our model include conduction to the substrate via the air gap under the microrobot, and via tethers. In the tethered case, the robot is stationary, therefore the laser beam is heating up both the robot and the surrounding substrate. In the case when an untethered microrobot is operated, it is inclined at a tilt angle to the substrate. In this case, a larger triangular prismatic-shaped air gap was defined under the actuator geometry, and conduction occurred through the air gap, as well as through direct contact of the dimple and feet to the substrate. The boundary conditions were modified to simulate the mobility of the robot via a constant temperature on the substrate. In our simulation, we used a total of 9305 hexahedron and tetrahedron mesh elements. Simulation runs to solve the transient thermal-mechanical process with 5000 data samples took typically 5 hours on a Core i7-600k @ 4Ghz computer.

Transient response simulations were run by setting volume heat generation as a step function input, and extracting temperature or displacement data for system identification. In a small-displacement linear approximation, a transfer function can be defined as $H(s) = \frac{Y(s)}{X(s)}$, in which X(s) is the volumetric heat generation in $pW/\mu m^3$(converted from the irradiance we mentioned), and Y(s) is the actuator displacement in μm. Using a unit step function volumetric heat generation, we can identify a first order model fit to data generated in either situation, leading to:

$$H_{tethered}(s) = \frac{0.280}{s+143.7}, \quad (18)$$

$$H_{untehtered}(s) = \frac{0.094}{s+556.8}. \quad (19)$$

Results indicate that the microrobot boundary conditions and operating environment have a considerable impact on its response. In particular, those ChevBots tethered to the substrate will have a steady state displacement and time constant equal to $0.280\,\mu m$ and $7\,ms$, respectively. Untethered ChevBots, on the other hand, experience a smaller static displacement $0.094\,\mu m$ and time constant $1.8\,ms$.

TABLE I. VALUES OF GEOMETRIC PARAMETERS AND MATERIAL CONSTANTS USED IN FEA SIMULATION OF CHEVBOTS.

l_b	Beam Length	200.25 (μm)
W_b	Beam width	5 (μm)
τ_b	Beam thickness	20 (μm)
α_b	Beam angle	2.860°
N	Beam number	12
ρ_{Si}	Density of Silicon	2328 $(kg \cdot m^{-3})$
E_{Si}	Si Young's modulus	165 (GPa)
k_{Si}	Si thermal conductivity	124 $(W \cdot m^{-1} \cdot ℃^{-1})$
C_{v-Si}	Si Specific heat constant	702 $(J \cdot kg^{-1} \cdot K^{-1})$
α_{Si}	Silicon thermal expansion	2.6e-6 $(℃^{-1})$
ρ_{air}	Density of Air	1.225 $(kg \cdot m^{-3})$
k_{air}	Air thermal conductivity	0.02624 $(W \cdot m^{-1} \cdot ℃^{-1})$
C_{v-air}	Air specific heat	716 $(J \cdot kg^{-1} \cdot K^{-1})$
h_{air}	Air convection constant	10 $(W \cdot m^{-2} \cdot K^{-1})$
τ_{air}	Thickness of Air Layer	2 (μm)

FEA can also calculate other important parameters of our model, including the actuator spring constant k. In particular, we applied $10\mu N$ force on the CTA, and recoded a shuttle deformation of $0.015\mu m$, resulting in a spring constant estimate $k = 645.5\,N/m$. Material and geometric FEA simulation parameters are detailed in Table I.

B. Velocity Prediction using 1D and 2D Models

Using the 1D and 2D dynamic models introduced in section III, we conducted simulations to predict the untethered microrobot motions on the substrate, with the help of time constants identified by the FEA. Values were further corrected after experiments (see section IV). The transfer function in eq. (19) was used to generate CTA actuator forces corresponding to pulsed laser irradiance levels. A 5kHz pulse signal of laser with peak energy (irradiance) 1.74e7 W/m^2 was input into the model and stick and slip Algorithm 1 was implemented in Simulink®. Simulation constants in Table II were obtained via a combination of FEA simulations, geometrical dimensions, while damping coefficients were approximated to correspond to overdamped responses consistent to Fig. 4. Simulation results from the 1D model are shown in Fig. 5. The plots depict a typical static-dynamic friction transition, and the resulting stick-slip causing a net velocity in the negative x direction, revealing that backward velocities of 55.59um/s can be achieved.

Ideally, because the ChevBot only have one actuator, their trajectories should align to a straight line, however, the presence of surface imperfections (particles, organics, etc.) on the substrate introduces uncertainty in friction/stiction constants that may vary between feet and dimple. Using the 2D model, we simulated different friction constants configurations represented by friction parameters of μ_s, μ_d. Simulation results are shown in Fig. 6. and reveal a high sensitivity of microrobot motion to surface conditions. ChevBot trajectories vary significantly in terms of turn radii, velocities, and direction of motion. In general, results indicate that the higher the friction coefficients, the faster the robot motions can be obtained, while the larger the friction imbalance, the smaller the turn radius.

TABLE II. VALUES OF GEOMETRIC PARAMETERS AND MATERIAL CONSTANTS USED IN 1D AND 2D DYNAMIC SIMULATION OF CHEVBOTS.

b	Damping	6.8e-5 (kg/s)
k_b	Spring constant	645.578 (N/m)
m_1	1-D mass of feet	1.095(μg)
m_2	1-D mass of frame	3.3054(μg)
h_d	Dimple height	20 (μm)
μ_s	Static friction constant	0.4
μ_d	Dynamic friction constant	0.33
k_v	Viscous constant	8.5e-7(Ns/m)
l_0	Original CTA length	170 (μm)
I	Angular Inertia	5.0957e-2 $(\mu g \cdot \mu m^2)$
m_{11}	Distributed mass on left feet	1.1324 (μg)
m_{12}	Distributed mass on right feet	1.1324 (μg)
m_2	Distributed mass on frame	1.5098 (μg)
r_{11}	Distance of left feet to center	50 (μm)
r_{12}	Distance of right feet to center	50 (μm)
θ_{11}	Configuration angle of left feet	1.5708 (rad)
θ_{12}	Configuration angle of right feet	-1.5708 (rad)

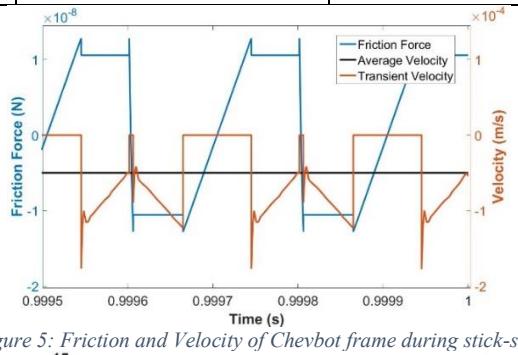

Figure 5: Friction and Velocity of Chevbot frame during stick-slip.

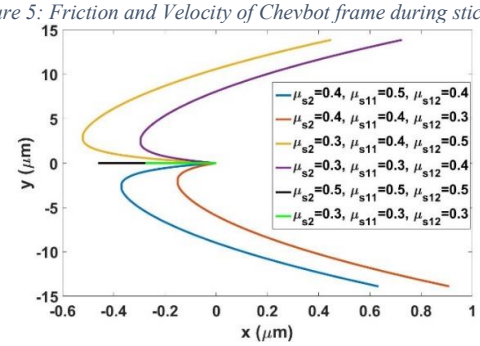

Figure 6 2D trajectories of the microrobot resulting from a combination of friction constants, assuming that μ_d is 90% of μ_s. Each trajectory is recorder over in 0.1 seconds, starting at the origin.

V. Experimental Validation

A. Experimental Instrument to Drive ChevBots

Experiments were realized with the help of a custom configured experimental instrument, shown in the schematic of Fig. 7. The components of the optical system include:

- Explorer One® Nd:YAG laser from Spectra-Physics, with 532nm wavelength, 2W Maximum power, 0.5-60 kHz repetition rate and 10 to 40ns pulse time width.
- A system of lenses, neutral density filters, beam splitters and mirrors to deliver laser energy to the microrobot.
- X-Y positioning stages from Newport: one 443 series and three 423 series, with two actuated by linear motor TRA25CC and two controlled manually.
- Tube lens, illuminator, beam splitter, NI Smart camera ISC-1772C for automated tracking and Pixelink CMOS camera for process visualization.
- A range sensor, LK-H008 from Keyence, to measure displacement of the tethered CTA actuator.

During the measurements, the laser beam can be operated under either continuous or burst mode. Continuous mode generates a series of pulses, while under burst mode, the user can specify the number of pulses within a burst and delay between each burst. For both cases, repetition rate of the fundamental pulses and diode current are adjustable. The average power of the laser is defined by diode current and repetition rate within each burst or during continuous mode.

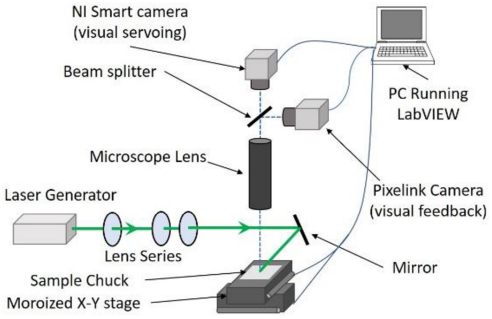

Figure 7 Laser delivery and vision acquisition schematic.

Two types of Chevbot laser irradiation experiments were conducted with tethered and untethered microrobots. In the case of the tethered ChevBot, only motion of the thermal actuator was studied. For the untethered microrobot, the goal was to initiate and record stick and slip motion of the whole microrobot on a silicon substrate with the overhead camera.

B. Tethered Chevbot Dynanic Response

In this configuration ChevBot's body was tethered to the (SOI) device layer thus its frame was stationary, and the actuator and feet are set into the motion upon laser irradiation. The purpose of these measurements was to characterize the actuator sub-micron displacements for specific boundary conditions and acquire results which could utilized for the system identification and validation of simulation results in section IV. The repetition rate of the laser was set to 1700Hz for maximum actuator displacement and the laser diode current was considered as input to system identification. The system's output was the displacement of the thermal actuator, measured by Keyence displacement sensor. A testing die was designed in such way that many tethered ChevBots are located at the edge of the die so that the displacement sensor has access to the leg of thermal actuator to acquire the dynamic measurement. The displacement sensor collected data at a sampling rate of 10kHz, as depicted in Fig. 8.

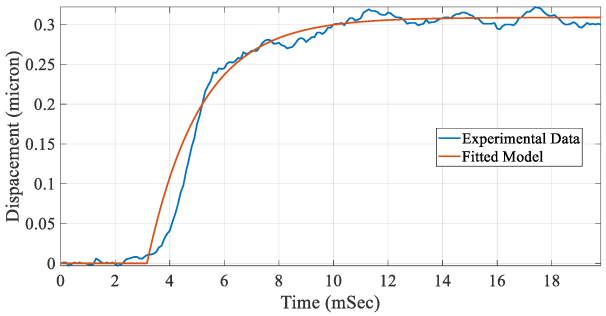

Figure 8 Laser power stimulus as input and ChevBot CTA actuator as output fitted to a first order transfer function displacement.

The transfer function identified experimentally is a ratio between laser irradiation, as measured indirectly via the laser diode current of the Explorer Nd:Yag unit, and the actuator displacement measured by the Keyence® sensor. As a result, the DC gain of this transfer function bears no similarity to that of the FEA model in section IV-A. However, the time constant of the model should be similar. The first order system identification results was:

$$H_{tethered}(s) = \frac{154.1}{s+524} \tag{20}$$

The system identification result shows the experimental time constant is about 2ms, while the FEA simulation for the tethered the boundary condition is 7ms. Through FEA, we concluded that the tethered robot boundary conditions have introduced more substrate thermal influence than the untethered case, leading to untethered robots time constants and displacements approximately 3 times faster/higher than tethered ones. As a result, we corrected our CTA simulation model estimates based on a time constant of 2ms.

C. Untethered Chevbot Velocity Measurements

In the second batch of experiments, assembled ChevBots were actuated on a silicon substrate by burst mode. The laser beam was focused onto the ChevBot with sufficient power to initiates gating motion, causing the robot to escape from the laser beam waist. At that point the microrobot loses power, the laser beam needs to be repositioned to track the motion of the robot. In a novel twist, we keep the laser beam position fixed, but we reposition the robot to the laser spot using a visual servoing scheme implemented by camera feedback [9]. The vision system processes the 640x480 pixel image and extracts the location of the microrobot with a pattern matching feature. An Image Jacobian was identified for visual servoing to bridge the mapping between robot feature positions and the stage displacement. In order to maintain the ChevBot in the center of the camera image, where the laser has been focused, visual servoing feedback provides current pixel location of ChevBots, compares it with the desired pixel location, and generates an error term to drive the stages.

Experiments were conducted with untethered Chevbots, confirming that the microrobot generates a fairly straight

trajectory in the defined backward direction, as shown in Fig. 9, where all trajectories begin from the origin for 0.1sec. The effect of different laser parameters on speed are summarized in Table III. The trajectory plots of the ChevBot are recorded using X and Y encoder readings of the stages while the microrobot is tracked. While most trajectories show straight components, the turning behavior suggests the microrobot encounters dust specks or unbalanced friction conditions. Depending on the geometry and surface condition of the dust, the microrobot may be forced to steer, or completely stop. The experimentally measured velocity of ChevBots under different laser configurations were compared to 1D simulation results, indicating general trend-wise agreement.

TABLE III. MEASURED AND SIMULATED VELOCITIES OF CHEVBOT UNDER VARYING LASER POWER CONDITIONS. 1D SIMULATIONS WERE CONDUCTED USING μS=0.4.

Test	*Pulses*	*Burst Delay*	*Average Power*	*Measured Velocity*	*Simulated Velocity-1D*
1	30	200ms	388~454mW	21.8μm/s	51.37μm/s
2	40	100ms	410~468mW	90.6μm/s	59.83μm/s
3	50	100ms	432~490mW	83.4μm/s	60.21μm/s
4	50	50ms	440~504mW	109.0μm/s	89.86μm/s

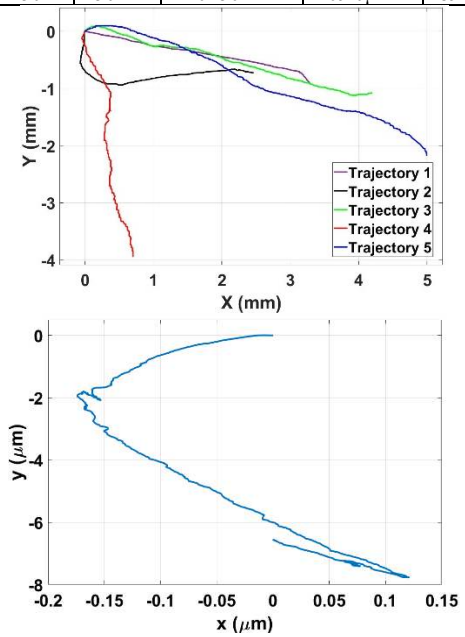

Figure 9 ChevBot's trajectories from 5 different experiments (top) in 1-2 minutes, and a randomized parameter 2D simulation result (bottom) in 0.1 seconds.

Finally, we randomized the friction constant for emulate varying surface condition of the substrate, with friction constants between 0.1 and 0.3. Simulation results shown in Fig. 9 (bottom) indicate that similar length trajectories to the experiment can be obtained through our fitted 2D model.

VI. CONCLUSION AND FUTURE WORK

In this paper we present a modeling methodology for laser-driven microrobots, based on a combination of Finite Element Analysis, lumped-model approximations, and experimentation with tethered and untethered prototypes. The ChevBot actuation principle is based on a complex multiphysics opto-thermo-mechanical conversion, and stick – slip friction contact with the substrate. FEA models were used to compare the displacement and time constants of the microrobots in tethered and untethered states. Tethered microrobots were subjected to laser pulses for system identification. The resulting first order thermal actuator models were fed into 1D and 2D stick and slip models to predict the velocity and orientation of the ChevBot operating on a flat Silicon substrate. Finally, a visual servoing scheme was employed to automatically track the robot and focus the laser beam. Motion tracking results indicate wide agreement with the simulation predictions and reveal that the microrobot is sensitive to robot-substrate friction conditions. In the future, the dynamic models will be used to prototype closed-loop controllers for microrobots, and to optimize their geometric and material parameters and improve performance.

REFERENCES

[1] B. J. Nelson, I. K. Kaliakatsos, and J. J. Abbott, "Microrobots for minimally invasive medicine." *Annual Review of Biomedical Engineering*, vol. 12, no. 1, p. 55, 2010.

[2] P. Ryan and E. Diller, "Magnetic Actuation for Full Dexterity Microrobotic Control Using Rotating Permanent Magnets," *IEEE TRANSACTIONS ON ROBOTICS,* vol. 33, no. 6, pp. 1398-1409, 2017.

[3] M. P. Kummer, J. J. Abbott, B. E. Kratochvil, R. Borer, A. Sengul and B. J. Nelson, "OctoMag: An Electromagnetic System for 5-DOF Wireless Micromanipulation," *IEEE Transactions on Robotics*, vol. 26, no. 6, pp. 1006-1017, 2010.

[4] E. Diller, S. Floyd, C. Pawashe and M. Sitti, "Control of Multiple Heterogeneous Magnetic Microrobots in Two Dimensions on Nonspecialized Surfaces," *IEEE Transactions on Robotics*, vol. 28, no. 1, pp. 172-182, 2012.

[5] C. Elbuken, M. B. Khamesee and M. Yavuz, "Magnetic levitation as a micromanipulation technique for MEMS," *2009 International Conference on Mechatronics and Automation*, Changchun, 2009, pp. 955-959.

[6] J. James, V. Iyer, Y. Chukewad, S. Gollakota and S. B. Fuller, "Liftoff of a 190 mg Laser-Powered Aerial Vehicle: The Lightest Wireless Robot to Fly," in *2018 IEEE International Conference on Robotics and Automation (ICRA)*, Brisbane, Australia, May 21-25, 2018.

[7] K. S. Ishii, W. Hu and A. T. Ohta, "Cooperative micromanipulation using optically controlled bubble microrobots," in *IEEE International Conference on Robotics and Automation*, Saint Paul, MN, USA, 2012.

[8] H. Chen, C. Wang, X. Li and D. Sun, "Transportation of MultipleBiological Cells Through Saturation-Controlled Optical Tweezers In Crowded Microenvironments," *IEEE/ASME Transactions on Mechatronics,* vol. 21, no. 2, pp. 888-899, 2016.

[9] R. Zhang, A. Sherehiy, Z. Yang, D. Wei, C. K. Harnett and D. O. Popa, "ChevBot – An Untethered Microrobot Powered by Laser for Microfactory Applications," to appear in *2019 International Conference on Robotics and Automation*, Montreal, Canada, 2019.

[10] L. Que, J.-S. Park and Y. B. Gianchandani, "Bent-beam electrothermal actuators-Part I: Single beam and cascaded devices," *Journal of Microelectromechanical Systems*, vol. 10, no. 2, pp. 247 - 254, Jun 2001.

[11] M. Tecpoyotl-Torres, J. Varona, A. A. Hamoui, J. Escobedo-Alatorre and J. Sanchez-Mondragón, "Polysilicon thermal micro-actuators for heat scavenging and power conversion," in *Proceedings* Volume 7043, High and Low Concentration for Solar Electric Applications III, San Diego, California, 2008.

[12] D.O. Popa, B.H. Kang, J.T. Wen, H.E. Stephanou, "Dynamic modeling and input shaping of thermal bimorph MEMS actuators," in *IEEE International Conference on Robotics and Automation*, Taipei, 2003.

[13] Liu, Y. F., Li, J., Zhang, Z. M., Hu, X. H., and Zhang, W. J.: Experimental comparison of five friction models on the same test-bed of the micro stick-slip motion system, Mech. Sci., 6, 15-28, 2015.

[14] *Fundamentals of Heat and Mass Transfer 7th Edition* by T. L. Bergman, et. al., John Willey & Sons, 2007.

[15] "Optical Absorption Coefficient Calculator," Brigham Young University Cleanroom, [Online]. Available: https://cleanroom.byu.edu/OpticalCalc#. [Accessed 15 9 2018].